Chinese Chemical Letters 35 (2024) 109465

Contents lists available at ScienceDirect

Chinese Chemical Letters

journal homepage: www.elsevier.com/locate/cclet

SOMO-HOMO level conversion in triarylmethyl-cored *N*-heterocyclic carbene-Au(I) complexes triggered by selecting coordination halogens

Le Zhang[1], Hui-Yu Xie[1], Xin Li, Li-Ying Sun*, Ying-Feng Han*

Key Laboratory of Synthetic and Natural Functional Molecule of the Ministry of Education, Xi'an Key Laboratory of Functional Supramolecular Structure and Materials, College of Chemistry and Materials Science, Northwest University, Xi'an 710127, China

ARTICLE INFO

Article history:
Received 4 November 2023
Revised 3 December 2023
Accepted 26 December 2023
Available online 30 December 2023

Keywords:
SOMO-HOMO conversion
N-heterocyclic carbenes
Aufbau and non-Aufbau
Electronic structure
Halogen atoms
Radical

ABSTRACT

Conventionally, organic radicals adhere to the Aufbau principle, the energy level of the singly occupied molecular orbital (SOMO) is not below the highest occupied molecular orbital (HOMO), but somewhat abnormal phenomena have appeared recently. In this study, we introduce a novel strategy by incorporating unique NHC-Au-X units into a tris(2,4,6-trichlorophenyl)methyl (TTM) system to create metal-involved open-shell complexes, denoted as TTM-NHC-Au-X (X = I, Br, or Cl). Density-functional theory calculations were used to predict an inversion in the energy of the SOMO and highest doubly occupied molecular orbital (HOMO) of TTM-NHC-Au-I, which is supported by experimental results. Organometallic radicals TTM-NHC-Au-X demonstrated distinct properties with different coordinated halides. The radical behaviors have been investigated by EPR, UV–vis spectroscopy and cyclic voltammetry, additional structural information provided by structurally comparing related the precursor complexes given by X-ray crystallography. TTM-NHC-Au-I with SOMO–HOMO conversion (SHC) features a highly thermal decomposition temperature up to 305 °C. Furthermore, the photostability of TTM-NHC-Au-I was found to be 75 and 23 times greater than that of TTM-NHC-Au-Br and TTM-NHC-Au-Cl, respectively. These findings provide valuable insights into the structural and electronic design principles governing the occurrence of SOMO–HOMO conversion in open-shell systems.

An energetic inversion of the singly occupied molecular orbital (SOMO) and the highest doubly occupied molecular orbital (HOMO) level is termed SOMO–HOMO conversion (SHC) [1–7]. The radicals with peculiar orbital energetics contribute their unique electronic properties, where the SOMO is not the highest occupied orbital in the species [8–11]. Recent extensive research on non-Aufbau electronic structures has led to conceptual developments in the switch for bond dissociation energy, transforming certain radical species into high-spin states through one-electron oxidation [5,8-16]. Specifically, SHC is associated with the unusual photostability or thermostability of organic radicals [12,13,15], and several SHC radicals exhibit high luminescence quantum yields, offering possibilities for their application in organic light-emitting diode devices [15,16]. SHC systems have been mainly achieved in organic radical molecules [17–28]. SHCs triggered by coordination to the metal center have been mostly limited in TEMPO-bound (TEMPO = 2,2,6,6-tetramethylpiperidine-l-oxy radical) dithiolate ligands [4,29,30]. Related metal-involved species are far less common, presumably because the methods that allow efficient control of SHC within metal complexes remain rare.

In this study, we describe a method for generating SHC within a series of NHC-Au (NHC = *N*-heterocyclic carbene) complexes based on molecular design. We focused on combining tris(2,4,6-trichlorophenyl)methyl (TTM) moiety and Au-NHC-halide units to realize a unique electronic structure by selecting coordination halides at the metal center. A series of radical-based functional materials have been achieved using the covalent attachment of different skeletons to TTM radicals [15,16,31-45]. Note that SHC could be performed when the HOMO orbital of the peripheral substituent is higher than the SOMO orbital of the TTM, and *vice versa* [46].

NHC-Au-X complexes exhibit interesting properties attributed to the characteristic electronic structure with different donating abilities of the halide ligands (X = I, Br or Cl) [47,48]. Although they have been rather frequently applied as catalysts in many organic reactions [49–54], their use in radical material systems is uncommon. Based on the density-functional theory (DFT) calculation results, the HOMO and LUMO energy levels of NHC-Au-X com-

* Corresponding authors.
E-mail addresses: lysun@nwu.edu.cn (L.-Y. Sun), yfhan@nwu.edu.cn (Y.-F. Han).
[1] These authors contributed equally to this work.

https://doi.org/10.1016/j.cclet.2023.109465
1001-8417/

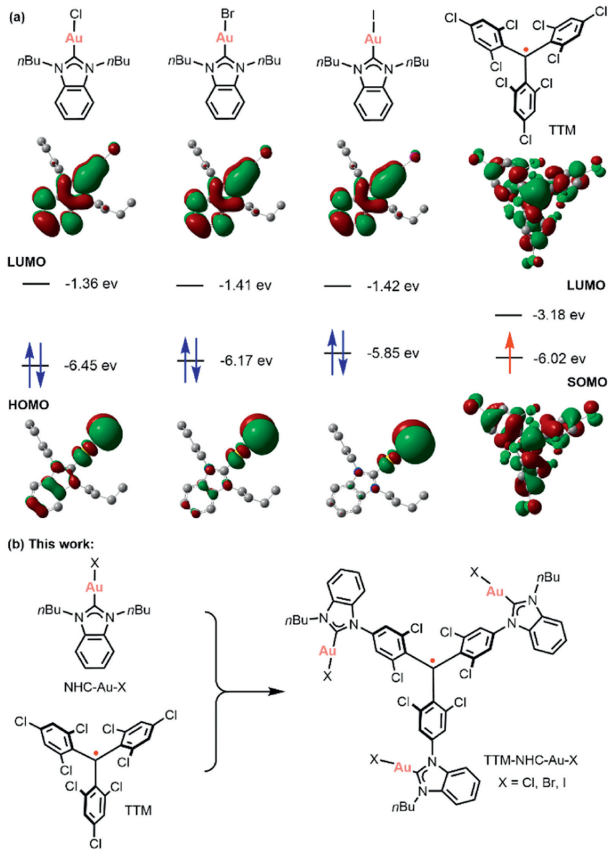

Fig. 1. (a) Spatial distribution of the frontier molecular orbitals and corresponding energy levels of NHC-Au-X (X = I, Br or Cl) and TTM calculated *via* DFT methods [(M06, UM06)/SDD (Au, Br, I) and 6–31G* (H, C, N, Cl)]. (b) The schematic synthesis of TTM-NHC-Au-X (X = I, Br or Cl).

plexes depend significantly on the electron-donating ability of the halide ligands (Fig. 1). The energy of the SOMO of TTM (−6.02 eV) is lower than the HOMO of NHC-Au-I (−5.85 eV), but higher than those in NHC-Au-Br (−6.17 eV) and NHC-Au-Cl (−6.45 eV). We believe that by introducing a unique NHC-Au-X unit in the TTM system, new classes of materials with SHC properties can be readily obtained through facile modification of coordinated halide atoms.

This study, successfully synthesized a series of TTM-centered gold carbene radicals TTM-NHC-Au-X (X = I, Br or Cl), and their precursors *α*-*H*TTM-NHC-Au-X. The electronic structure, photophysical properties, electrochemical studies, and stability of these newly obtained organometallic radicals were investigated, along with their single-crystal X-ray diffraction (XRD) analysis. The iodine atoms on the gold centers allow for an SHC phenomenon, that tunes the property of the molecule. However, SHC was not observed when the bromide or chloride was used as coordinated ligands. Notably, TTM-NHC-Au-I showed significantly higher thermal and photostability than its Br/Cl counterparts.

According to our molecular design, three NHC precursors, benzimidazolium-substituted triarymethyl compounds **2a-c** were designed and synthesized from tris[4-(1*H*-benzimidazolyl)−2,6-dichlorophenyl]methyl (**1**) following Scheme 1. Treatment of 2a-c with [AuCl(THT)] to generate trinuclear gold(I) complexes *α*-*H*TTM-NHC-Au-X (**3a-c**) in anhydrous dichloromethane under the exclusion of light in good yields. Compounds **2a-c** and **3a-c** were verified using nuclear magnetic resonance (NMR) spectroscopy (^{1}H and ^{13}C{^{1}H}) and high-resolution electrospray ionization (HR-ESI) mass spectrometry (Figs. S1-S27 in Supporting information). In the ^{13}C NMR spectrum of complexes **3a-c**, which displays decreasing upfield shifts of the C_{NHC} resonance from 187.4 ppm (**3a**) > 181.4 ppm (**3b**) > 178.1 ppm (**3c**). These different chemical shifts reveal the characteristic donating ability of halide atoms, where the more upfield shift corresponds to weaker donor fragments [47,48]. Subsequently, complexes **3a-c** were treated with tetrabutylammonium hydroxide (TBAH) in anhydrous THF to generate the corresponding anions. Furthermore, through oxidation with tetrachloro-*p*-chloranil, three organometallic radical complexes **4a-c** containing different halogen atoms were isolated after workup (Scheme 1). The complexes **4a-c** were characterized through HR-ESI, element analysis, ultraviolet-visible (UV–vis) adsorption spectroscopy, and single-crystal XRD analysis (**4b** and **4c**). The radical feature in **4a-c** was confirmed using electron paramagnetic resonance (EPR) spectroscopy.

The solid-state **3a-c** molecular structures were unambiguously determined through single-crystal XRD experiments (Fig. 2a and Figs. S28-S30 in Supporting information). The Au-X (X = I, Br or Cl) **3a-c** bond lengths were found to decrease as the electronegativity of the halogen atoms increased, with an order of 2.532(4)–2.557(2) Å (**3a**) > 2.382(10)–2.396(11) Å (**3b**) > 2.266(2)–2.300(3) Å (**3c**) (Table S1 in Supporting information).

X-ray crystallographic analyses of **4b** and **4c** revealed that each isolated complex consists of a TTM radical center and three NHC-Au-X (X = Br or Cl) units at the periphery (Fig. 2b, Figs. S31 and S32 in Supporting information), which agrees with the configuration inferred from HR-ESI mass spectrum in the liquid phase. Noted that the C_1-C_2, C_1-C_3 and C_1-C_4 bond lengths of **4b** (1.510(10) Å, 1.503(10) Å and 1.499(10) Å) are significantly shorter than those of 3b (1.586(11) Å, 1.545(11) Å and 1.526(11) Å). In contrast, the C_2-C_1-C_3, C_2-C_1-C_4 and C_3-C_1-C_4 bond angles of **4b** (120.7(7)°, 119.0(7)° and 120.3(7)°) are bigger than those of **3b** (116.5(7)°, 115.6(7)° and118.7(8)°) (Fig. 2b, and Table S1 in Supporting information). Additionally, the central carbon atom C_1 of radical **4b** is sp^2 hybridized and coplanar with three adjacent carbon atoms bonded to it (C_2, C_3, and C_4). However, the central carbon atom C_1 of complex **3b** is sp^3 hybridized and non-coplanar with the adjacent carbon atoms. Similar changes were observed between complexes **3c** and **4c** (Figs. S30 and S32, Table S1 in Supporting information). These observations revealed the radical character of organometallic complex **4b**.

The neighbouring intermolecular Au···Au distances of **3b** and **4b** are in the range of 3.26–3.80 Å and 3.25–3.72 Å, respectively, indicating the presence of Au···Au interactions in the solid states (Figs. S29 and S31). Similar intermolecular Au···Au interactions were observed in the structures of complexes **3a**, **3c** and **4c** (Figs. S28, S30 and S32). Additionally, intermolecular X···π interactions evidently existed in such systems (Figs. S28-S32).

All solution samples of radical complexes **4a-c** for UV–vis absorption, photoluminescence (PL) excitation and emission properties were investigated. Fig. 3a and Fig. S33 (Supporting information) show that two new characteristic absorption maxima at around 380 and 560 nm were observed after the generation of radicals in contrast to their precursor's **3a-c**. There is a slight wavelength shift due to the distinct electronegativity of metal coordination atoms. For instance, a set of strong short wavelength absorption at 388 nm (**4a**), 380 nm (**4b**), 386 nm (**4c**), and a low-lying band at 567 nm (**4a**), 564 nm (**4b**), 563 nm (**4c**), respectively. For the PL spectra, the maximum fluorescence peaks were located at 592 nm (**4b**) and 589 nm (**4c**), whereas radical **4a** underwent an obvious red-shift at 607 nm (average 20 nm) in toluene solution (Fig. 3b, Figs. S33d and S34 in Supporting information).

Complexes **4a-c** were doped into poly(methyl methacrylate) (PMMA) films to investigate the photophysical properties of the radicals in solid-state thin films, and the emission spectra and quantum yields of the formed thin films were measured. In contrast to those in solution, complexes **4a** (603 nm) and **4b** (585 nm) exhibited slight blue shifts, and complex **4c** (609 nm) has a wider

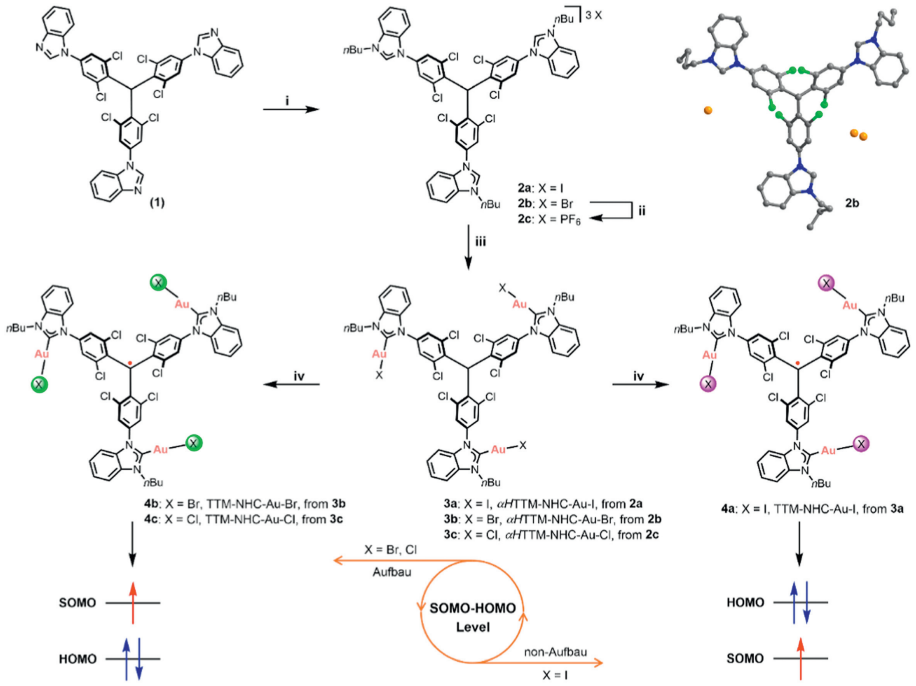

Scheme 1. Synthesis of ligands **2a-c**, complexes **3a-c** and radicals **4a-c**. (i) nBuBr or nBuI, DMF, 120 °C, 36 h; (ii) NH_4PF_6, MeOH, r.t., 24 h; (iii) K_2CO_3, AuCl(THT), dry DCM, in dark, r.t., 36 h; (iv) TBAH, tetrachloro-p-chloranil, dry THF, in dark, r.t., 7 h. Ligand **2b** is also shown as a crystal structure. Hydrogen atoms, and molecules of the solvent of crystallization are omitted for clarity. Color code: Cl, green; Br, brown green; C, grey; N, blue.

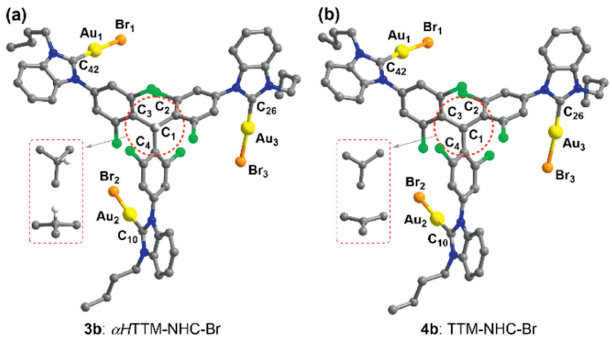

Fig. 2. X-ray crystal structures of (a) complex **3b** and (b) radical **4b**. Hydrogen atoms, the partial center structure, and molecules of the solvent of crystallization are omitted for clarity. Color code: Au, yellow; Cl, green; Br, brown green; C, grey; N, blue; H, white. Selected bond parameters in Å and deg: **3b**, C_1-C_2 1.586(11), C_1-C_3 1.545(11), C_1-C_4 1.526(11), Au_1-C_{42} 1.999(8), Au_2-C_{10}, 1.990(8), Au_3-C_{26}, 1.976(9), Au_1-Br_1 2.3875(9), Au_2-Br_2 2.3817(10), Au_3-Br_3 2.3959(11), C_2-C_1-C_3 116.5(7), C_2-C_1-C_4 115.6(7), C_3-C_1-C_4 118.7(8); **4b**, C_1-C_2 1.510(10), C_1-C_3 1.503(10), C_1-C_4 1.499(10), Au_1-C_{42} 1.990(11), Au_2-C_{10}, 1.977(11), Au_3-C_{26}, 2.001(10), Au_1-Br_1 2.3591(13), Au_2-Br_2 2.3644(14), Au_3-Br_3 2.3939(15), C_2-C_1-C_3 120.7(7), C_2-C_1-C_4 119.0(7), C_3-C_1-C_4 120.3(7).

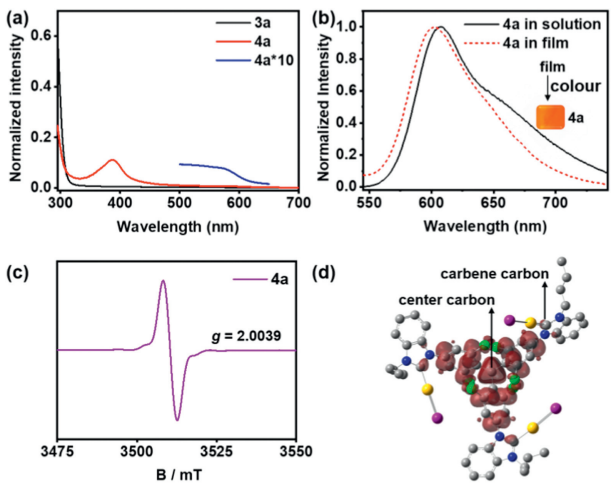

Fig. 3. (a) UV–vis absorption spectra of **3a** and **4a** in CH_2Cl_2 ($c = 10^{-5}$ mol/L, 298 K). (b) Normalized emission spectra of **4a** in $PhCH_3$ ($c = 10^{-4}$ mol/L, 298 K, solid lines) and **4a** (2 wt%) doped in PMMA film (298 K, dash lines). (c) EPR spectra of **4a** in CH_2Cl_2 ($c = 10^{-3}$ mol/L, 298 K). (d) Spin density distribution of **4a** calculated *via* DFT methods [UM06/SDD (Au, I) and 6–31G* (H, C, N, Cl)]. Color code for (d): Au, yellow; Cl, green; I, purple; C, grey; N, blue.

red shift of 18 nm (Fig. 3b and Fig. S34 in Supporting information). The photoluminescence quantum yields (PLQY) of the spin-coated **4a-c** films were 1.0% (**4a**), 1.8% (**4b**), and 1.4% (**4c**), respectively.

The magnetic properties of radicals **4a-c** were measured at room temperature by EPR. There intense and broad EPR signal peaks with $g = 2.0039$ (**4a**), 2.0041 (**4b**), and 2.0044 (**4c**) were recorded, each featuring a typical sign of one unpaired electron (Fig. 3c and Fig. S35 in Supporting information).

For a deeper understanding of the radical's electronic distribution and molecular orbitals, quantum chemical calculations were performed using DFT. The results demonstrate that the spin density is distributed from the center to the periphery, with the highest at the center carbon site (*ca.* 0.837) and a small spin density at the carbene carbon atom (*ca.* 0.003) (Fig. 3d and Fig. S35 in Supporting information). The molecular orbital calculation results exhibit that the SOMO of all radical complexes **4a-c** is delocalized over the TTM radical unit with a minor extension to the halogen gold carbene pendants. Meanwhile, the HOMO is mainly concentrated in the halogen gold carbene segments (Fig. 4). Specifically, the SOMO orbital energy level in radical **4a** is lower than that of the HOMO, indicating a clear violation of the Aufbau principle (Fig. 4a). The calculated spin density of radical **4a** also reflects the SOMO orbital (286 α-spin) and the corresponding LUMO orbital (290 β-spin). Conversely, the SOMO orbitals of **4b** and **4c** are higher than the HOMO orbitals, which align with the Aufbau principle (Figs. 4b and c). The SOMO orbital of **4a** is located in the lower energy orbital of the inner layer, which may result in lower reactivity and higher stability than **4b** and **4c**. We repeated

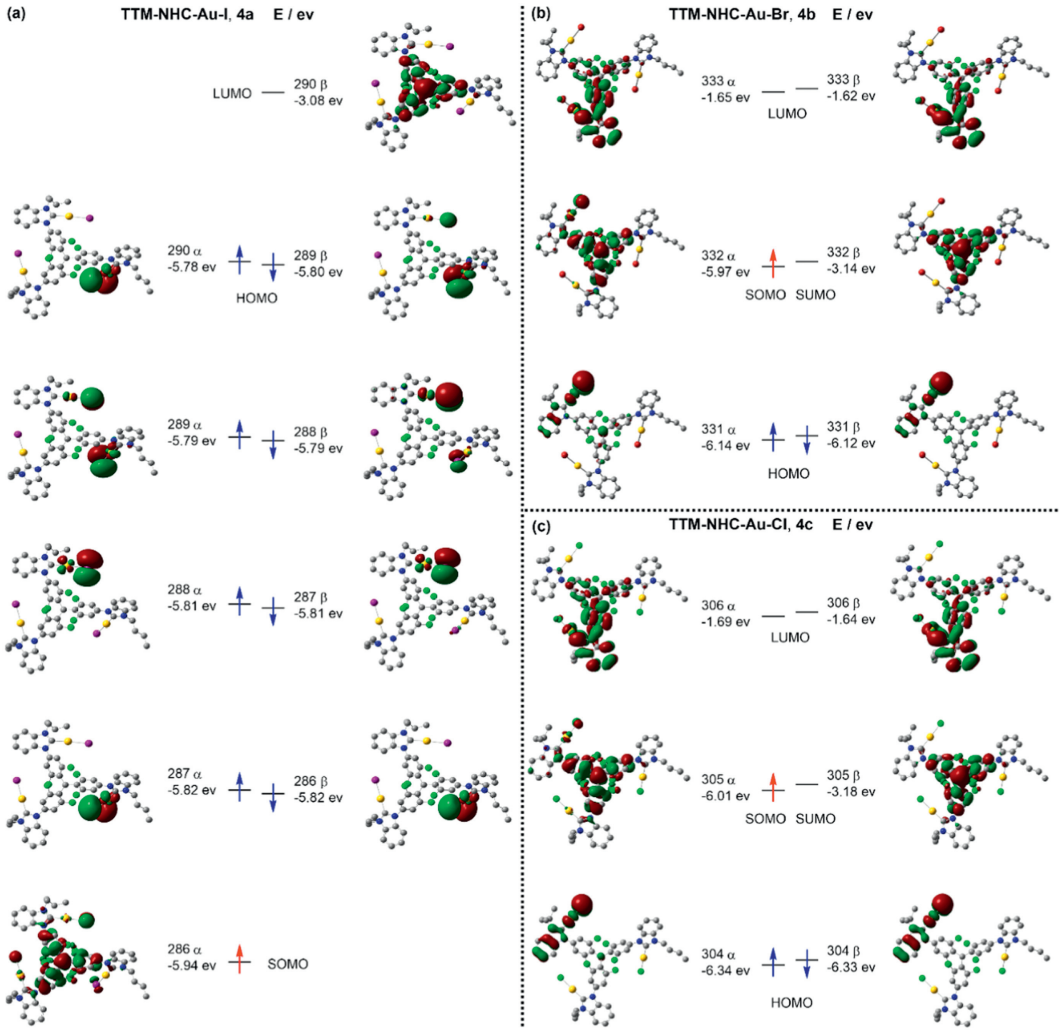

Fig. 4. Spatial distribution of the frontier molecular orbitals and corresponding energy levels of (a) **4a**, (b) **4b**, and (c) **4c** calculated *via* DFT [UM06/SDD (Au, Br, I) and 6–31G* (H, C, N, Cl)].

the process using another method to validate the accuracy of the theoretical calculations, and the results were consistent with the expected outcomes. The DFT calculation [UB3LYP/SDD (Au, I), 6–31G* (H, C, N, Cl)] confirmed that SOMO–HOMO conversion can be achieved for **4a** (Fig. S36 in Supporting information).

Since the redox experiment is an essential characterization method for confirming the orbital turnover of radicals [15,46], a series of redox properties were measured to gain deeper insights into the electronic characteristics of the complexes. The electrochemical behavior of the metal carbene radicals **4a**-**c**, the radical center (TTM), and the isolated fragment molecule (NHC-Au-I) are presented graphically (Fig. 5a and Fig. S37 in Supporting information). Strikingly, the radicals **4a**-**c** has high electrochemical stability, and no significant decomposition was observed after 50 scanning cycles. The cyclic voltammetry (CV) spectra of **4b** and **4c** display two pairs of redox potentials, with a reduction peak at −0.63 V (**4b**), −0.62 V (**4c**), and an oxidation peak at +1.15 V (**4b**), +1.16 V (**4c**), respectively, which correspond to the −0.89 V and +1.11 V values observed in TTM (Fig. S37). For **4a**, a reduction and oxidation peak close to those of **4b** and **4c** appears at −0.70 V and +1.01 V. Additionally, two new oxidation peaks occur at +0.20 V and +0.54 V, which are distinct features unobserved in **4b** and **4c**. Notably, these new **4a** peaks are excellently interconnected with the NHC-Au-I pendants, which show oxidation potentials at +0.09 V and +0.50 V (Fig. 5a). This evidence implies that **4a** exhibits different redox be-

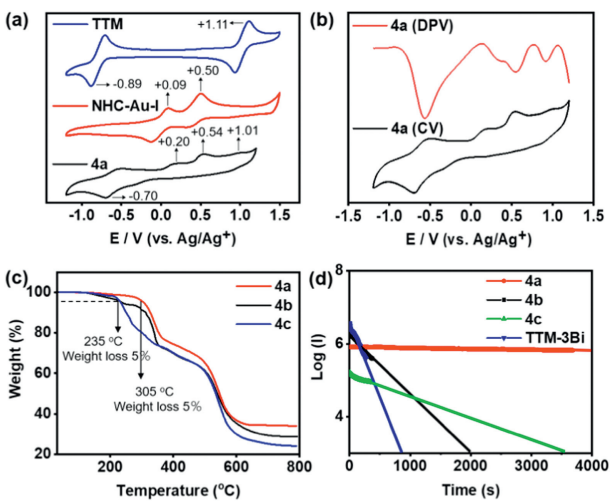

Fig. 5. (a) Cyclic voltammograms of TTM (blue), NHC-Au-I (red), and **4a** (black) in CH_2Cl_2 (nBu_4NPF_6, 100 mV/s, $c = 10^{-3}$ mol/L). (b) Differential pulse voltammogram and Cyclic voltammogram of **4a** in CH_2Cl_2 (nBu_4NPF_6, 100 mV/s, $c = 10^{-3}$ mol/L). (c) Thermal gravimetric analysis (TGA) of **4a**-**c** under N_2. (d) Plots showing emission decay of **4a**-**c** in $PhCH_3$ under continuous excitation at $\lambda_{ex} = 380$ nm ($c = 10^{-4}$ mol/L, 298 K).

havior compared to **4b** and **4c**, further explaining their distinct electronic structures. Moreover, the differential pulse voltammogram (DPV) experiment also reveals four and two oxidation waves for radicals **4a** and **4b**/**4c**, respectively (Fig. 5b and Fig. S37). Therefore, both CV and DPV data confirm that radical **4a** does not conform to the Aufbau principle, which is consistent with the DFT results.

The thermal and photochemical stability of **4a-c** were surveyed under a nitrogen atmosphere. The thermal properties of **4a-c** were researched with thermogravimetric analysis (TGA). Radical **4a** exhibited no degradation until attaining a temperature of 305 °C, whereas radicals **4b** and **4c** had lower decomposition temperatures at approximately 235 °C (Fig. 5c and Fig. S38 in Supporting information). Additionally, the degeneration of their fluorescence intensity was investigated through continuous excitation at $\lambda_{ex} = 380$ nm in a diluted toluene solution and compared with tris[4-(1*H*-benzimidazolyl)−2,6-dichlorophenyl]methyl radical (TTM-3Bi). Fig. 5d shows that the fitted half-time ($t_{1/2}$) of radical **4a** is 2.65×10^4 s, a value nearly two orders of magnitude larger than that of TTM-3Bi, a stronger photostability radical compound [32]. In contrast, the degenerate lifetime of the fluorescence intensity for **4b** and **4c** significantly decreases to 3.55×10^2 s and 1.13×10^3 s, respectively. The results above indicate that the non-Aufbau behavior exhibited by radical **4a** confers superior stability compared to the Aufbau behavior observed in radicals **4b** and **4c**, which is consistent with previous reports for such derivatives [15].

In summary, we designed, synthesized, and characterized a new series of metal-carbene complexes of persistent TTM core-based radicals. Theoretical calculation and experiment results proved that the SOMO and HOMO orbital energy levels of radicals **4a-c** could be adjusted by altering coordination halogen to metal atoms, and the organometallic radical complexes with non-Aufbau (**4a**) and Aufbau (**4b**, **4c**) electronic structures were readily accessible. This strategy provides a new technique for synthesizing organometallic radical complexes that violate the Aufbau principle. Additionally, TTM-NHC-Au-I based on realizing the SOMO–HOMO converted unique electronic structure showed significantly higher thermal and photostability than its Br/Cl counterparts. Significantly improving the thermal- and photostability of radicals will expand their practical applications. Given the efficient synthetic method established in this study, different kinds of organometallic radicals with other coordinated ligands and diverse NHC skeletons can be envisioned. Thus, further research into their potential applications in multifunctional materials with optical and magnetic responses is required.

Declaration of competing interest

The authors declare that they have no known competing financial interests or personal relationships that could have appeared to influence the work reported in this paper.

Acknowledgments

The authors gratefully acknowledge financial support from the National Natural Science Fund for Distinguished Young Scholars of China (No. 22025107), Shaanxi Fundamental Science Research Project for Chemistry & Biology (No. 22JHZ003), the National Youth Top-notch Talent Support Program of China, Xi'an Key Laboratory of Functional Supramolecular Structure and Materials, and the FM&EM International Joint Laboratory of Northwest University.

Supplementary materials

Supplementary material associated with this article can be found, in the online version, at doi:10.1016/j.cclet.2023.109465.

References

[1] N. Bohr, Z. Physik. 13 (1923) 117–165.
[2] J. Nakazaki, M.M. Matsushita, A. Izuoka, et al., Tetrahedron. Lett. 40 (1999) 5027–5030.
[3] J. Nakazaki, Y. Ishikawa, A. Izuoka, et al., Chem. Phys. Lett. 319 (2000) 385–390.
[4] T. Kusamoto, S. Kume, H. Nishihara, J. Am. Chem. Soc. 130 (2008) 13844–13845.
[5] R. Murata, Z. Wang, M. Abe, Aust. J. Chem. 74 (2021) 827–837.
[6] L. Abella, J. Crassous, L. Favereau, et al., Chem. Mater. 33 (2021) 3678–3691.
[7] S. Kasemthaveechok, L. Abella, M. Jean, et al., J. Am. Chem. Soc. 144 (2022) 7253–7263.
[8] M.M. Matsushita, H. Kawakami, T. Sugawara, M. Ogata, Phys. Rev. B 77 (2008) 195208.
[9] A. Kumar, M.D. Sevilla, J. Phys. Chem. B 122 (2018) 98–105.
[10] R. Murata, Z. Wang, Y. Miyazawa, et al., Org. Lett. 23 (2021) 4955–4959.
[11] Y. Li, Z. Ding, Q. Mu, et al., Dalton Trans. 52 (2023) 384–393.
[12] S. Kasemthaveechok, L. Abella, M. Jean, et al., J. Am. Chem. Soc. 142 (2020) 20409–20418.
[13] S. Kasemthaveechok, L. Abella, J. Crassous, et al., Chem. Sci. 13 (2022) 9833–9847.
[14] A. Rajca, C. Shu, H. Zhang, et al., Photochem. Photobiol. 97 (2021) 1376–1390.
[15] H. Guo, Q. Peng, X.K. Chen, et al., Nat. Mater. 18 (2019) 977–984.
[16] Z. Cui, A. Abdurahman, X. Ai, et al., CCS Chem. 2 (2020) 1129–1145.
[17] T. Sugawara, H. Komatsu, K. Suzuki, Chem. Soc. Rev. 40 (2011) 3105–3118.
[18] G. Gryn'ova, M.L. Coote, J. Am. Chem. Soc. 135 (2013) 15392–15403.
[19] P. Franchi, E. Mezzina, M. Lucarini, J. Am. Chem. Soc. 136 (2014) 1250–1252.
[20] Y. Wang, H. Zhang, M. Pink, et al., J. Am. Chem. Soc. 138 (2016) 7298–7304.
[21] S.M. Rivero, R. Shang, H. Hamada, et al., Bull. Chem. Soc. Jpn. 94 (2021) 989–996.
[22] T. Sugawara, M.M. Matsushita, J. Mater. Chem. 19 (2009) 1738–1753.
[23] H. Komatsu, M.M. Matsushita, S. Yamamura, et al., J. Am. Chem. Soc. 132 (2010) 4528–4529.
[24] G. Gryn'ova, D.L. Marshall, S.J. Blanksby, et al., Nat. Chem. 5 (2013) 474–481.
[25] A. Kumar, M.D. Sevilla, J. Phys. Chem. B 118 (2014) 5453–5458.
[26] T. Tsuchiya, Y. Katsuoka, K. Yoza, et al., ChemPlusChem 84 (2019) 1659–1667.
[27] A. Tanushi, S. Kimura, T. Kusamoto, et al., J. Phys. Chem. C 123 (2019) 4417–4423.
[28] E. Cho, V. Coropceanu, J.L. Brédas, J. Am. Chem. Soc. 142 (2020) 17782–17786.
[29] T. Kusamoto, S. Kume, H. Nishihara, Angew. Chem. Int. Ed. 49 (2010) 529–531.
[30] G. Grynóva, M.L. Coote, C. Corminboeuf, Wiley Interdiscip, Rev. Comput. Mol. Sci. 5 (2015) 440–459.
[31] A. Obolda, M. Zhang, F. Li, Chin. Chem. Lett. 27 (2016) 1345–1349.
[32] Y. Gao, W. Xu, H. Ma, et al., Chem. Mater. 29 (2017) 6733–6739.
[33] X. Ai, F. Li, Chin. Sci. Bull. 62 (2017) 4123–4130.
[34] X. Ai, E.W. Evans, S. Dong, et al., Nature 563 (2018) 536–540.
[35] A. Abdurahman, T.J.H. Hele, Q. Gu, et al., Nat. Mater. 19 (2020) 1224–1229.
[36] Y. Zhao, A. Abdurahman, Y. Zhang, et al., CCS Chem. 3 (2021) 938–947.
[37] X. Li, Y.L. Wang, C. Chen, et al., Nat. Commun. 13 (2022) 5367.
[38] Y. Hattori, T. Kusamoto, H. Nishihara, Angew. Chem. Int. Ed. 53 (2014) 11845–11848.
[39] Y. Hattori, T. Kusamoto, H. Nishihara, Angew. Chem. Int. Ed. 54 (2015) 3731–3734.
[40] Y. Hattori, T. Kusamoto, T. Sato, et al., Chem. Commun. 52 (2016) 13393–13396.
[41] Y. Ogino, T. Kusamoto, Y. Hattori, et al., Inorg. Chem. 56 (2017) 3909–3915.
[42] Y. Hattori, R. Kitajima, R. Matsuoka, et al., Chem. Commun. 58 (2022) 2560–2563.
[43] S. Kimura, R. Matsuoka, S. Kimura, et al., J. Am. Chem. Soc. 143 (2021) 5610–5615.
[44] S. Kimura, M. Uejima, W. Ota, et al., J. Am. Chem. Soc. 143 (2021) 4329–4338.
[45] X. Hou, G.T. Nguyen, T. Xu, et al., Chem. Eur. J. 28 (2022) e202200687.
[46] Z. Chen, F. Li, Chem. Res. Chin. U. 38 (2022) 798–802.
[47] M.V. Baker, P.J. Barnard, S.K. Brayshaw, et al., Dalton Trans. 1 (2005) 37–43.
[48] H.V. Huynh, S. Guo, W. Wu, Organometallics 32 (2013) 4591–4600.
[49] S. Ibáñez, M. Poyatos, E. Peris, Organometallics 36 (2017) 1447–1451.
[50] Y. Tang, I. Benaissa, M. Huynh, et al., Chem. Int. Ed. 58 (2019) 7977–7981.
[51] A. Kumar, C. Singh, H. Tinnermann, et al., Organometallics 39 (2020) 172–181.
[52] R.P. Herrera, M.C. Gimeno, Chem. Rev. 121 (2021) 8311–8363.
[53] D. Nugegoda, N.V. Tzouras, S.P. Nolan, et al., Inorg. Chem. 61 (2022) 18802–18809.
[54] P. Gao, J. Xu, T. Zhou, et al., Angew. Chem. Int. Ed. 62 (2023) e202218427.